



Cite this: *Chem. Sci.*, 2017, 8, 4696

Received 31st March 2017  
Accepted 30th May 2017

DOI: 10.1039/c7sc01441d

rsc.li/chemical-science

# Emerging plasmonic nanostructures for controlling and enhancing photoluminescence

Jeong-Eun Park, Jiyeon Kim and Jwa-Min Nam \*

Localised surface plasmon resonance endows plasmonic nanostructures with unique, powerful properties such as photoluminescence enhancement, which is a phenomenon based on the interaction between light and a metal nanostructure. In particular, photoluminescence modulation and enhancement are of importance to many research fields such as photonics, plasmonics and biosensing. In this minireview, we introduce basic principles of plasmonic-nanostructure photoluminescence and recently reported plasmonic nanostructures exhibiting surface-enhanced fluorescence and direct photoluminescence, with one-photon photoluminescence being of particular interest. Gaining insights into these systems not only helps understand the fundamental concepts of plasmonic nanostructures but also advances and extends their applications.

## 1. Introduction

When the dimensions of metallic nanostructures are smaller than the wavelength of incident light, the strong resonant interaction between electromagnetic radiation and localised surface charges of plasmonic nanostructures induces coherent non-propagating oscillation of surface plasmons denoted as localised surface plasmon resonance (LSPR). This unique light-matter interaction results in sub-wavelength localisation of the electromagnetic field, creating a plasmonic nanoantenna and thus endowing these nanoparticles with extraordinary properties, including surface-enhanced Raman scattering (SERS), photoluminescence (PL) enhancement ability and photothermal/photocatalytic activity.<sup>1</sup> Among these properties, PL enhancement is particularly

interesting, being potentially applicable in photonics and nanobiotechnology.<sup>2–5</sup> Surface-enhanced fluorescence (SEF) denotes a representative phenomenon of plasmon-induced PL enhancement, with the first report of a metal-fluorophore interaction dating back to 1974.<sup>6</sup> Plasmonic nanostructures enhance fluorescence by improving the brightness, photostability and photodegradation resistance of fluorophores in the near-field. These phenomena are mainly ascribed to increase in the emitter radiative decay rate, with decreased lifetime of the excited state of a fluorophore.<sup>7–9</sup> This coupling of fluorescence enhancement with increased photostability has attracted the attention of researchers from various fields, including the detection of chemical/biological analytes and understanding of microenvironments, offering opportunities to control and enhance fluorescence in an efficient manner. The PL of metals, first observed in 1969 by Mooradian,<sup>10</sup> does not suffer from photobleaching or photoblinking, which distinguishes it from that of organic dyes or quantum dots.

Department of Chemistry, Seoul National University, Seoul 08826, South Korea.  
E-mail: jmnam@snu.ac.kr



*Jeong-Eun Park received her B.S. degree in chemistry from Pusan National University in Busan, Korea in 2010. She joined the laboratory of Professor Jwa-Min Nam at Seoul National University as a Ph. D. student in 2010. Her major interests include the synthesis and optics of plasmonic nanostructures.*



*Ji Yeon Kim received her B. S. and M. S. degrees in chemistry from Yonsei University in 2013 and 2015, respectively. She joined the laboratory of Professor Jwa-Min Nam at Seoul National University as a Ph. D. student in 2016. Her current research focus is the direct photoluminescence from plasmonic nanoparticles.*



However, this phenomenon was rarely studied prior to 2000 due to its low quantum yield and limited understanding. Since then, the PL of plasmonic nanostructures, particularly of nanorods, has attracted increased attention, and its relationship to LSPR has been recognised.

In this minireview, we describe the fundamentals of PL from plasmonic nanostructures and emerging photoluminescent plasmonic nanostructures. Based on the nature of the light-emitting substance, we divide the paper into two parts, namely SEF and direct PL of plasmonic nanostructures, with one-photon PL being of particular interest. For each part, we briefly explain the principles and recent advances and describe future perspectives.

## 2. Surface-enhanced fluorescence

### 2.1. Principles of SEF

The origin of SEF is the fluorophore–LSPR interaction, with the corresponding energy transfer at short distances being mainly dominated by dipole–dipole interactions, which is known as the Förster resonance energy transfer (FRET) (Fig. 1a). When LSPR bands overlap with the fluorophore absorption spectrum, FRET induces enhanced plasmon-to-fluorophore (or *vice versa*) energy transfer, resulting in a slight increase of fluorescence intensity (the pink arrows in the top scheme of Fig. 1a). If the LSPR energy matches that of the fluorophore emission, FRET results in fluorescence quenching (the grey arrow in the top scheme of Fig. 1a) due to the intrinsically large plasmon absorption cross-section, with a typical distance to avoid signal quenching exceeding 5 nm.

At longer distances, the effect of FRET becomes insignificant, since its efficiency decays as  $1/r^6$  (where  $r$  denotes the plasmon–fluorophore separation distance), resulting in the

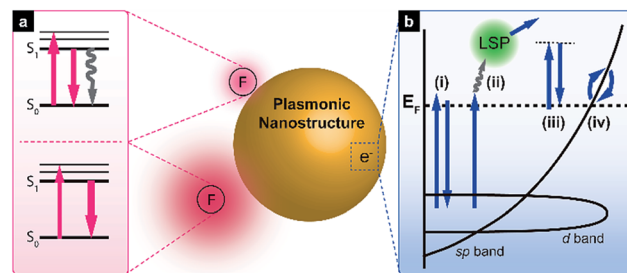
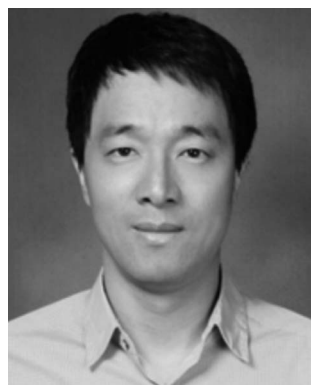


Fig. 1 Schematic illustration of controlling and enhancing PL with plasmonic nanostructures. (a) Jablonski diagram illustrating fluorescence signal changes when emitters are close to or at a short distance from plasmonic nanoparticles. (b) Simplified band diagram of gold showing a possible electronic transition for direct PL.

domination of the Purcell effect, which scales with  $1/r^3$  (the bottom scheme in Fig. 1a). The Purcell factor, *i.e.*, the enhancement of the spontaneous emission rate of a fluorescent molecule by its environment, originates from the strong local near field, so-called hot spots, generated by neighbouring plasmonic nanostructures. Since the local density of optical states (LDOS) is proportional to the square of the local electric field strength, dipoles experiencing a strong local near field can emit more photons in this mode, which ideally corresponds to the maximum LSPR wavelength. Thus, the fluorescence emission rate is eventually enhanced due to LDOS alteration, and the Purcell effect can be maximised if the LSPR band overlaps primarily with the fluorescence emission band. For an in-depth description of the underlying mechanism, please refer to previously published reports.<sup>3,11–13</sup>

### 2.2. Emerging plasmonic nanostructures for SEF

In the last 10–20 years, researchers have focused on simple fluorescence signal enhancement using nanoantennae. Recent investigations have attempted to maximise and characterise fluorescence enhancement at a single-nanoantenna level, with top-down approaches such as focused ion beam lithography being preferred due to allowing reliable hot-spot design and creation. When the antenna-in-box is exposed to a fluorophore solution, dye molecules can reside in its gap junction, while the surrounding nanoaperture box effectively screens background dye molecules diffusing away from the junction, resulting in a 1100-fold fluorescence enhancement (Fig. 2a).<sup>14</sup> Additionally, the corresponding molecular dynamics was analysed using fluorescence correlation spectroscopy to quantify the detection volume and brightness per emitter. As a result, detection volumes as small as 58 zL and count rates above 300 kHz per molecule were determined, significantly exceeding the values achieved in the absence of the above antenna. Nanoparticle-on-mirror (or patch antenna) is another promising nanostructure comprising a metal disk and a metal plane with emitters situated in a vertical gap. Unlike lithographically fabricated systems, sub-10 nm gaps can be easily realised in this case, allowing high Purcell factors to be achieved.<sup>15–17</sup> For example, an Au film/Ag nanocube patch antenna achieved one of the highest enhancement factors (above 2000) reported so far (Fig. 2b).<sup>18</sup>



Professor Jwa-Min Nam received his Ph.D. in chemistry from Northwestern University and worked as a postdoctoral fellow at the University of California, Berkeley. He joined the Department of Chemistry at Seoul National University in 2006, and is currently a full professor in the chemistry department. He received the Chinese Academy of Sciences Fellowship for International Scientists, the Presidential

Young Scientist Award from the President of the Republic of Korea, Young Inorganic Chemist Award from the Korean Chemical Society, and Victor K. LaMer award from the American Chemical Society. He serves as an executive advisory board member for Small Methods (Wiley-VCH) and an editorial board member for ChemNanoMat (Wiley-VCH). His research interests include design and synthesis of plasmonic nanostructures, plasmonically engineered nanoprobe for biosensing, bioimaging and therapeutics, nanoparticle-tethered lipid bilayers, and cell–nanostructure interfaces.





**Fig. 2** Plasmonic nanostructures used for PL enhancement. (a) Plasmonic 'antenna-in-box' platform; (b) plasmonic Au film with a Ag nanocube patch antenna containing embedded dyes; (c) Ag-coated atomic force microscopy tip with a single quantum dot; (d) dimeric Au NP assembly synthesised utilising a DNA origami technique; (e) Au nanomatryoshka composed of a gold core, an interstitial nanoscale SiO<sub>2</sub> layer containing a dye, and a Au shell; (f) core-shell Ag-silica nanoparticles with a distance-controlled photosensitizer. Images were reproduced with permission from (a) ref. 14, Copyright 2013 Nature Publishing Group; (b) ref. 18, Copyright 2014 Nature Publishing Group; (c) ref. 20, Copyright 2016 American Chemical Society; (d) ref. 24, Copyright 2015 American Chemical Society; (e) ref. 26, Copyright 2014 American Chemical Society; (f) ref. 37, Copyright 2016 American Chemical Society.

The above design also allows simultaneous directional emission and high radiative quantum efficiency. Time-resolved fluorescence characterisation of the film-coupled metal nanocube system with emitters embedded in the dielectric gap region revealed that the spontaneous emission lifetime was reduced from 600 ns to less than 0.7 ns. The observed emission rate enhancement and high quantum efficiency ( $>0.5$ ) resulted in a maximum radiative rate enhancement of  $\sim 1000$ , maintaining a spatially uniform collection efficiency of 84%. The patch antenna design was further extended to the use of quantum dots, achieving a spontaneous emission rate enhancement of 880 and a total fluorescence enhancement of 2300.<sup>19</sup> The PL enhancement of a single quantum dot was also investigated using a Ag-coated atomic force microscopy tip exhibiting a well-defined LSPR, with PL modulated by the spectral overlap and the distance between the quantum dot and the tip (Fig. 2c).<sup>20</sup> As this distance decreased, single-photon emission transformed into multiphoton emission with a reduced lifetime, which was attributed to energy transfer from the quantum dot to the silver tip, with the local electric field of the tip further enhancing emission intensity.

Another way to achieve signal enhancement is presented by the bottom-up approach, which is cost-effective and relatively simple in processing. Single plasmonic nanoparticles can act as efficient

nanoantennae for SEF, as exemplified by nanorods, which feature a highly tuneable LSPR band and a strong local field at the end of their tips due to the lightning rod effect. When Au nanorods immobilised on a glass surface are exposed to fluorophore solution, excitation and emission rate enhancement factors of  $\sim 130$  and  $\sim 9$  are achieved, respectively, resulting in an overall 1100-fold enhancement, which is comparable to that obtained using top-down methods.<sup>21</sup> The above enhancement distinctly decreases when the SPR wavelength differs from the excitation wavelength, indicating the importance of matching these wavelengths. Another systematic study of distance- and plasmon-wavelength-dependent fluorescence, utilising silica-coated Au nanorods and infrared dyes, demonstrated a maximum ten-fold enhancement when the nanorod plasmon maximum overlapped with the dye absorption band.<sup>22</sup> Plasmonic coupling between nanoparticles results in a strong near field at the nanogap junction separating them. For instance, a self-assembled Au nanosphere dimer with a 6 nm gap exhibiting a more affordable and simpler design achieved a 600-fold fluorescence enhancement.<sup>23</sup> A similar nanoantenna with reduced interparticle distances was developed using a specially designed DNA origami template, accomplishing a maximum 5000-fold fluorescence enhancement and single-emitter detection at 25  $\mu\text{M}$  (Fig. 2d).<sup>24</sup> A strong near field can be generated using a single nanoparticle. Compared to the strong plasmonic coupling



between nanoparticles, interior-gap-based plasmonic couplings provide more consistent and reproducible enhancement properties.<sup>25–28</sup> Nanomatyoshkas are one example of structures exhibiting such couplings, featuring a concentric core and shell separated by a dielectric gap. The strong core-shell coupling leads to highly concentrated radiation in the gap region and further increases the fluorescence of emitters contained therein. A systematic finite difference time domain simulation performed by screening various parameters resulted in a maximum enhancement factor of well above  $\sim 1500$  for the gold matryoshka.<sup>29</sup> The experimental results obtained for this structure by other researchers reveal that wavelength-dependent fluorescence enhancement is maximised when the LSPR wavelength overlaps with the excitation wavelength of embedded fluorophores.<sup>26</sup> The maximum fluorescence signal is obtained at maximal near-field enhancement, leading to a  $\sim 16$ -fold intensity increase (Fig. 2e). Recently, a gold nanostructured array has been demonstrated to enhance a second near-infrared (NIR-II; 1000–1400 nm) fluorescence signal of Ag<sub>2</sub>S quantum dots,<sup>30</sup> resulting in a  $\sim 100$ -fold fluorescence enhancement at an emission wavelength of 1200 nm.

Besides conventional fluorescence enhancement, different emitter types, *e.g.*, upconversion nanoparticles (UCNPs) or phosphors have also been employed. Improving the characteristics of UCNP emitters, which can be excited with low-energy light sources, is interesting in view of their relatively low quantum yield.<sup>31–33</sup> NaYF<sub>4</sub>:Yb<sup>3+</sup>,Er<sup>3+</sup> UCNPs were assembled near one end of Au nanorods, matching their longitudinal LSPRs with the phosphor excitation wavelength of 977 nm.<sup>34</sup> When UCNP-nanorod heterodimers were excited with light polarised along the longitudinal axis of the Au nanorod, a two-fold luminescence signal intensity increase was observed in single-particle measurements. The same nanocrystals hybridised with Ag nanowires were harnessed as a potential power source for solar cells in optically transparent free-standing silk fibroin films,<sup>35</sup> with precise and reliable distance control between UCNPs and nanoantennae achieved using polyelectrolyte multilayers as tuneable dielectric spacers.<sup>36</sup> Once the LSPR absorption wavelength was matched with the excitation wavelength of UCNPs, a maximum 23-fold enhancement was accomplished using an 8 nm spacer. Recently, plasmons have been demonstrated to affect phosphorescence enhancement. As these transitions occur very slowly, emission is observed up to several hours after excitation. As an example, photosensitisers (Rose Bengal) attached to the surface of Ag-silica core-shell nanoparticles generated singlet oxygen (<sup>1</sup>O<sub>2</sub>), the phosphorescence of which at 1275 nm was enhanced by 7 times (Fig. 2f).<sup>37</sup>

### 3. Direct one-photon photoluminescence of plasmonic nanostructures

#### 3.1. Fundamentals of plasmonic nanostructure photoluminescence

When excitation energy is matched with the intrinsic interband transition energy of metals, the above transition occurs, with d-band electrons excited into the sp-band (Fig. 1b, pathway

(i)).<sup>10,38</sup> For metallic gold, the direct recombination of sp-band electrons with d-band holes preferentially occurs near the *L*- and *X*-symmetry points of the Brillouin zone of its face-centred cubic (fcc) crystal structure, resulting in luminescence at 510 and 650 nm, respectively.<sup>39</sup> However, the excited electrons mainly decay *via* non-radiative relaxation processes such as electron-phonon and phonon-phonon scattering, thereby yielding a very low quantum efficiency ( $\sim 10^{-10}$ ). Although local field enhancement by a rough metal surface was reported to enhance PL,<sup>40</sup> photoluminescent metal nanoparticles have begun to attract attention only recently. Au nanorods show PL intensities several orders of magnitude higher than those of other metals due to the lightning rod effect, which is interpreted as local field enhancement by mechanisms such as SEF and SERS.<sup>41</sup> In particular, Au nanospheres with different maximum scattering wavelengths exhibit PL spectra where the peak positions of PL and scattering shift similarly.<sup>42</sup> Based on these results, one can propose a new mechanism, in which excited d-band holes recombine with sp-band electrons and excite particle plasmons that subsequently undergo radiative decay (Fig. 1b, pathway (ii)). Lithographically defined gold nanostructures such as nanodiscs, nanotriangles, and nanorods exhibit shape-dependent PL spectra.<sup>43</sup> Since the direct recombination of d-band holes and sp-band electrons is affected by material nature and temperature, but not by its shape, a similar mechanism was suggested. When LSPR energy matches that of the interband transition, both this transition and LSPR excitation occur (with the relative contributions of these processes being unknown), and excited plasmons emit light. In some cases, the excitation energy does not overlap with that of the interband transition, which can be rationalised in a number of ways, *e.g.*, by electronic Raman scattering (also denoted as electronic inelastic scattering), which postulates the excitation of an sp-band electron to a virtual state with subsequent relaxation (Fig. 1b, pathway (iii)).<sup>44–46</sup> Temperature-dependent SERS measurements allowed the anti-Stokes backgrounds in the corresponding spectra to be analysed, with thermally activated inelastic light scattering proposed as a result. Similar to this result, the SERS spectra from self-assembled monolayers on nanostructured gold surfaces show a broad continuum background, which can be explained by plasmon-modulated PL.<sup>39</sup> In contrast to wavelength-independent electronic Raman scattering, another model proposes wavelength-dependent intra-band transitions of sp-band electrons to explain excitation-wavelength-dependent PL spectra (Fig. 1b, pathway (iv)).<sup>47</sup> Still plasmons play an important role, helping spatially localise electrons to surface areas around strong near-field regions or out-couple the radiation to the far-field.<sup>44</sup> Although the exact underlying mechanism of PL cannot be clarified further, the crucial role of LSPR in plasmonic nanostructure PL has now been recognised. Initially, most studies focused on determining quantum yields of simple nanoparticles or modulating PL spectra by controlling polarisation angles or excitation wavelengths. Currently, further investigations of theoretical background of the PL mechanism<sup>45,48</sup> and plasmon-enhanced PL phenomena are underway.



### 3.2. Engineering the direct photoluminescence of plasmonic nanostructures

The precise modulation or further enhancement of the direct PL of plasmonic nanostructures is a subject of ongoing debate. Owing to the highly tuneable LSPR and the lightning rod effect, Au nanorods are the most widely studied nanoparticles, exhibiting the strong PL with a quantum efficiency of  $\sim 10^{-6}$ .<sup>47,49–51</sup> Therefore, when studying the PL of other nanoparticles, the observed PL intensity is often compared with that of Au nanorods to confirm signal enhancement. The aspect ratio of the rod or the excitation wavelength can also be adjusted to obtain a PL signal of the desired wavelength. Au nanobipyramids show quantum yields one order of magnitude higher than those of Au nanorods, which is attributed to local field enhancement around the sharper ends, supposedly causing a more pronounced lightning rod effect (Fig. 3a).<sup>51</sup> In a similar way, the local field enhancement and better PL-LSPR

spectral overlap of Au nanocubes result in PL quantum yields exceeding those of Au nanorods upon irradiation at the same excitation wavelength.<sup>52</sup> PL enhancement has been also studied for plasmonically coupled nanostructures obtained by attaching a single nanostructure to a metal film to form gap plasmons or cavities. When an Au nanoparticle was placed on an  $\text{Al}_2\text{O}_3$ -coated Au film, a significantly increased signal near the gap-plasmon resonance was detected for excitation at 633 nm, as compared to the case when these nanoparticles were absent (Fig. 3b).<sup>53</sup> Irradiation at 633 nm efficiently excited the gap plasmon mode, inducing a strong electric field near the particle-substrate junction together with interband absorption near the X point of the Brillouin zone. In the same way, although Ag nanowires and Au films exhibit weak PL on their own, their combination (featuring a 6 nm dielectric spacer) resulted in an intensified PL signal.<sup>54</sup> Taking into account the similarity between scattering and PL spectra, a PL mechanism featuring radiative damping of gap plasmons was proposed,

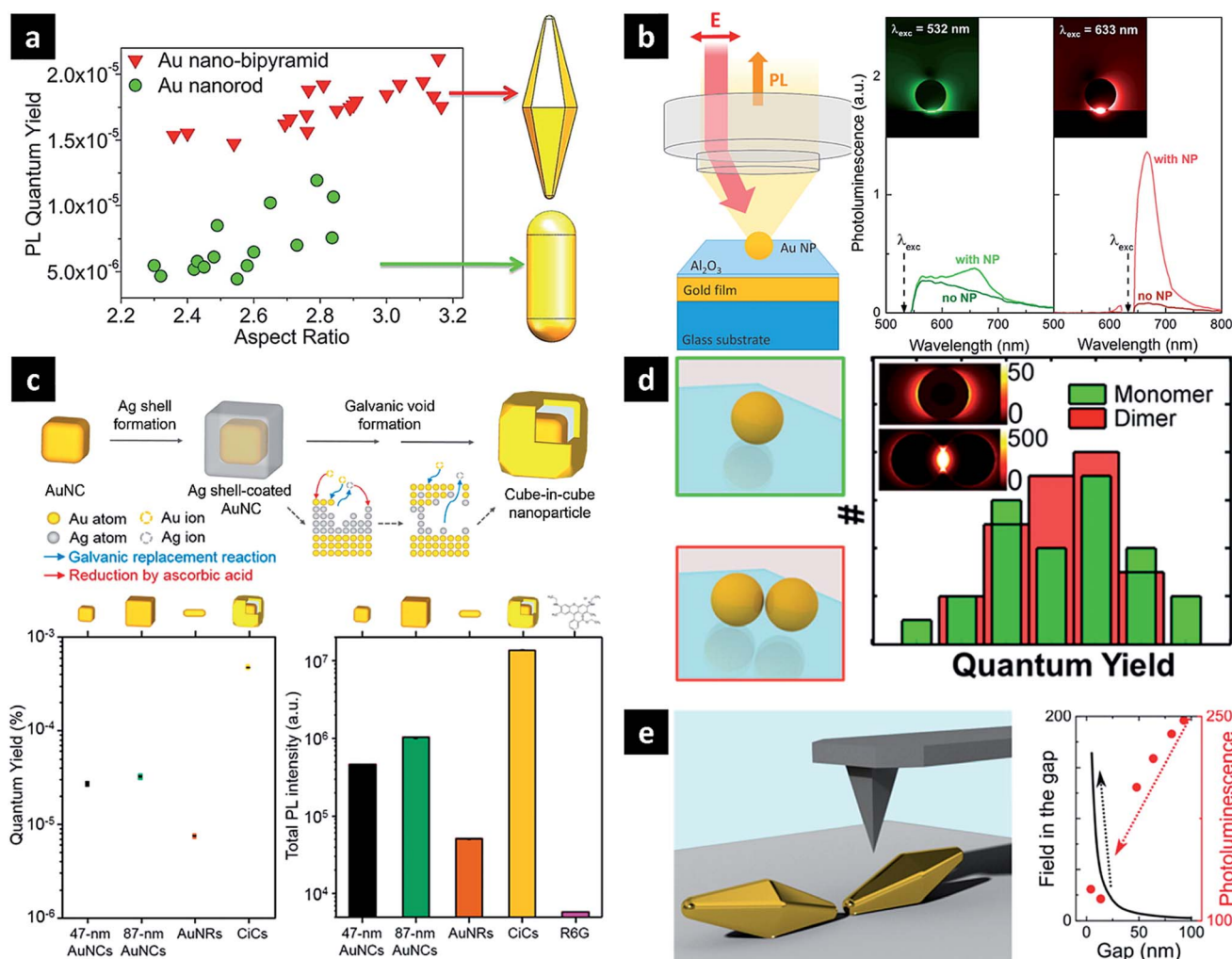


Fig. 3 Plasmonic nanostructures for direct one-photon PL. (a) Au nanobipyramid and nanorod; (b) Au nanoparticle coupled with Au film with an interstitial  $\text{Al}_2\text{O}_3$  layer; (c) cube-in-cube nanoparticle featuring an Au nanocube, a nanogap, and a cubic nanoshell; (d) Au nanoparticle dimer with close tips (e) Au nanopyramid dimer assembled edge-to-edge. Images were reproduced with permission from (a) ref. 51, Copyright 2015 American Chemical Society; (b) ref. 53, Copyright 2014 American Chemical Society; (c) ref. 27, Copyright 2016 American Chemical Society; (d) ref. 56, Copyright 2015 American Chemical Society; (e) ref. 57, Copyright 2016 American Chemical Society.

with the Ag nanowire acting as an efficient antenna for enhanced laser absorption and PL emission. PL enhancement has also been achieved as a result of photon emission by deliberate inelastic tunnelling.<sup>55</sup> For instance, upon laser illumination, the small gap between the sharp Au tip and the Au substrate used in scanning tunnelling microscopy activates hot electron tunnelling to enhance PL. Based on the analysis of the total photon emission profile, the contributions of ordinary light-induced electron–hole recombination and radiative plasmon decay to PL can be distinguished, revealing the dominance of photon emission by hot electrons slightly above the Fermi level *via* plasmonic modes created by inelastic tunnelling.

Plasmonic coupling may also be induced within a single nanoparticle. Cube-in-cube (CiC) nanoparticles of a core-gap-shell type with an engineerable interior nanogap were synthesised using the galvanic void formation process, composed of replacement/reduction and void formation steps (Fig. 3c).<sup>27</sup> In this structure, the core-shell plasmonic coupling generates two plasmon modes, rationalised using the plasmon hybridisation model. In this model, parallel coupling of two dipoles increases the total dipole moment, resulting in a super-radiant plasmon mode, whereas antiparallel coupling results in sub-radiant behaviour. While the core Au nanocube was known to exhibit the highest PL intensity and quantum yield reported for metallic nanostructures, the corresponding parameters of 9 nm-gap CiC NPs are 31 and 16 times higher than those of Au nanocubes, respectively. In particular, large Au nanocubes with a size similar to that of 9 nm-gap CiC NPs exhibited markedly lower intensities, indicating the important role of the inner gap for enhanced PL. This enhancement was rationalised by the super-radiant plasmon mode, which significantly increased the radiative damping of the corresponding plasmons. The concept of super-radiance, initially introduced to describe the cooperative emission of organic fluorophores, can be successfully applied to plasmonic nanostructures, with the empirical quantum efficiency being similar to the enhanced radiative damping rate obtained by calculations. Thus, CiC NPs exhibit the highest luminescence intensity and quantum yield ever reported for metallic NPs.

Some studies have shown that plasmonic coupling has no effect on PL enhancement, or stronger coupling actually decreasing the PL signal. Au nanodimers composed of two nanospheres were prepared, and their PL was compared with that of the monomeric structure. The dimer showed two distinct PL peaks, with wavelengths similar to those observed in the corresponding scattering spectrum, even though the lower-energy peak showed a much higher intensity in the latter case. Interestingly, the intensity increase of the PL signal mirrored the corresponding increase in absorption, and therefore, the quantum yield of the dimer was found to be similar to that of its constituent monomers (Fig. 3d).<sup>56</sup> Thus, despite the formation of a strong local electric field between two nanoparticles, a similar quantum yield was obtained for dimeric and monomeric structures, contradicting the results of previous studies that ascribed increased PL to local field enhancement. When the distance between the tips of two Au nanobipyramids was varied using AFM, the scattering signal intensity increased

with decreasing interparticle distance, while the PL intensity concomitantly decreased (Fig. 3e).<sup>57</sup> This anticorrelation was interpreted by a theoretical model describing intrinsic d-band hole recombination probabilities and the field strength inside nanostructures. The effect of near-field coupling on PL was systematically investigated using sparse arrays of gold nanoparticles with varying size and separation fabricated by electron beam lithography.<sup>58</sup> The emission wavelengths, line shapes, and quantum yields were distinctly dependent on particle size and separation, which was attributed to different LSPR modes. Notably, this coupled array system exhibits a much larger coupling distance than systems mentioned earlier.

Although coupling strength may affect PL enhancement, as described in Section 3.1, the overlap of excitation wavelength with that of the interband transition and LSPR is critical to PL enhancement, necessitating the exploration and verification of this phenomenon under various conditions.<sup>39,41</sup>

## 4. Emerging applications

Since PL can be used to detect or sense targets of interest, its main applications include sensing, detection, and imaging. In the case of SEF, signal enhancement is achieved by bringing the dye close to the nanoparticles, with the presence of targets detected by quenching or recovering the fluorescence signal of the attached dye. Lithographically fabricated systems can be used as substrates or chips for *in vitro* signal enhancement. Typical enzyme-linked immunosorbent assays with dye-modified antibodies on plasmonic Au nano-island film enhance near-infrared fluorescence signal intensities up to 100-fold, providing a much broader dynamic range (reaching into the femtomol regime) and remarkable signal-to-noise ratios compared to glass and commercial nitrocellulose substrates (Fig. 4a).<sup>59</sup> This platform was successfully used for the early detection of a cancer biomarker (carcinoembryonic antigen) in the sera of mice with a xenograft tumour. Since *in vivo* applications utilise nanoparticles in preference to other substrates, the observed fluorescence enhancement factors are relatively low, up to several dozens. Nevertheless, nanoparticles offer the advantages of easy delivery, good biocompatibility and multifunctionality, showing potential for further utilisation. A straightforward method involves direct contact between dielectric shell (SiO<sub>2</sub>)-coated plasmonic nanoparticles and dye molecules, resulting in a fluorescence decrease when fluorescence quenchers are introduced. The dye can be attached to the surface *via* a direct covalent bond, generating a strong fluorescence signal. When a reagent capable of fluorescence quenching is introduced, *e.g.*, Cu<sup>2+</sup>, it can be detected based on decreased fluorescence. In addition, a second reagent such as pyrophosphate can be added to the system to eliminate the effect of the first reagent by binding it in the form of a complex, and the observed signal recovery can be used to determine the presence of this second reagent (Fig. 4b).<sup>60</sup> Pyrophosphate, a by-product of nucleic acid amplification, was utilised to detect microRNA with the aid of rolling circle amplification, achieving a detection limit of 8.4 pM for let-7d microRNA. The dye can be brought in close contact with the nanoparticle surface bearing



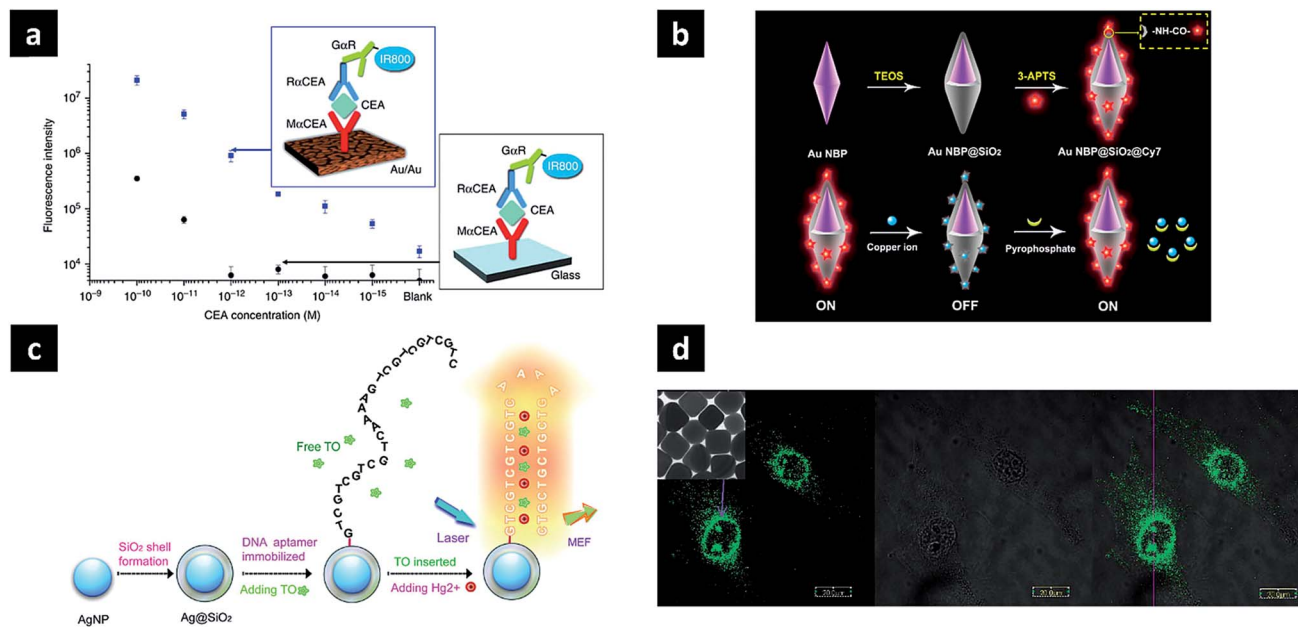


Fig. 4 Applications of photoluminescent plasmonic nanostructures. (a) Au nano-island film as SEF substrate for protein detection; (b) silica-coated Au nanobipyramids exhibiting distance-dependent fluorescence enhancement for microRNA detection; (c) silica-coated Ag nanoparticle for Hg<sup>2+</sup> sensing; (d) enhanced PL of Au nanocubes for bioimaging. Images were reproduced with permission from (a) ref. 59, Copyright 2011 Nature Publishing Group (b) ref. 60, Copyright 2016 American Chemical Society; (c) ref. 61, Copyright 2015 Nature Publishing Group; (d) ref. 52, Copyright 2010 American Chemical Society.

targets, the presence of which can be detected by signal enhancement. When T-rich DNA aptamers are grafted onto the SiO<sub>2</sub> shell, they are stabilised by Hg<sup>2+</sup> to form a hairpin-structure T-Hg<sup>2+</sup>-T complex. Then, the introduced dye can intercalate double-helix DNA, being located close to the surface, which results in fluorescence enhancement (Fig. 4c).<sup>61</sup>

As for direct PL, the plasmonic nanostructure itself can act as a label-free sensor. For example, the monitoring of catalytic reactions on the surface of plasmonic nanostructures has been reported at a single-nanoparticle level. Au nanorods can oxidise ethanol under visible light irradiation, featuring hot electron transfer from excited nanorods to dissolved oxygen and subsequent ethanol oxidation by the generated electron-deficient nanorods. The competition for electrons between the catalytic reaction and PL results in luminescence quenching upon oxidation.<sup>62</sup> In addition, corresponding molecular sensing and cell imaging applications have also been demonstrated. Biological molecule binding can be efficiently detected based on optical refractive index changes occurring in the vicinity of nanostructures, which induces a shift of PL peak wavelength.<sup>63</sup> Au nanocubes, known to exhibit stronger PL than spherical or rod-type Au nanoparticles, can be utilised as optical labels in cell imaging (Fig. 4d).<sup>52</sup>

## 5. Challenges and prospects

So far, we have introduced the underlying principles and recently reported discoveries pertaining to the design, synthesis and use of photoluminescent plasmonic nanostructures. The fine-tuning of these nanostructures can maximise the

enhancement factor, achieving values of up to several thousands. However, the applications of photoluminescent plasmonic nanostructures are not extensive, which is attributed to poor mechanistic understanding and the relatively weak signal, offering poor controllability and significantly lower enhancement for practical applications. Better and clearer understanding of the PL enhancement mechanism, designing the nanostructures, and the synthetic realisation of targeted nanostructures with high structural precision and high yield are key challenges in this field. Considering the Brownian motion or fluctuation in solution, only some dye molecules momentarily placed in a strong electric field produce an enhanced signal, while the remaining molecules do not effectively experience the strong near-field. Further, even nm-range change in position of dye molecules can largely affect the degree of signal enhancement. Therefore, precise control of molecular positioning is required, *e.g.*, placing dye molecules in a specific position or the utilization of ultra-nanogaps to maximise fluorescence enhancement. Besides, if long-term optical stability is achieved with the help of plasmons, the fluorescence signal can be monitored for an extended time period, overcoming the currently largest challenge of photobleaching for long-term or 3D tracking. The enhancement of NIR fluorescence, which exhibits relatively low quantum yields and poor stability, is another challenge that needs to be solved to enable practical use. Recently, several researchers have reported that the NIR-II window (1000–1400 nm) provides several advantages over the conventional NIR-I window (750–900 nm) for biomedical applications, including greater penetration depth (more suitable for *in vivo* application) and reduction of autofluorescence





(resulting in reduced background intensity and lower laser radiation doses).<sup>64,65</sup> Moreover, the NIR-II window is a relatively safe spectral region, owing to its higher value of maximum permissible exposure to laser radiation.<sup>66</sup> Thus, efficient enhancement of fluorescence in the NIR-II region can aid the practical utilisation of the above technology.

The direct PL of plasmonic nanostructures still leaves much room for improvements. The primary difficulty in this field is low quantum yield, and the highest quantum yield achieved by a plasmonic nanostructure is on the order of  $10^{-4}$ , which is two orders of magnitude lower compared to that of organic fluorophores or quantum dots. The absence of methods for fabricating plasmonic nanostructures with strong PL are compromising the in-depth exploration of the PL of plasmonic nanostructures. Structural collapse even after prolonged laser exposure is not allowed in order to exploit the non-photobleaching and non-photoblinking properties, which are great advantages of the direct PL of plasmonic nanoparticles. Once a deeper understanding of the underlying mechanism is obtained, various methods of manipulating and controlling PL will be developed. Owing to the large absorption cross-section of single plasmonic nanostructures, their total PL intensity can be much higher than those of conventional organic fluorophores such as rhodamine 6G, offering potential applications as optical labels.<sup>27</sup> The PL of other plasmonic materials such as copper or aluminium is worth exploring as an opportunity of developing cost-effective PL nanoprobe. Improving the PL quantum yield to the values comparable to that of fluorophores or quantum dots would make plasmonic nanostructures as strong candidates for next-generation optical labels in the fields of optics, sensing, and imaging. Potential applications of the direct PL can be further expanded to diverse systems: monitoring of biological and catalytic processes, optical stimuli of optoelectronic devices, and photoactive nanorobots or nanoactuators.

## Acknowledgements

J.-M. N. was supported by a National Research Foundation of Korea (NRF) grant funded by the Korea government (Ministry of Science, ICT & Future Planning (MSIP)) (No. 2016R1A2A1A05005430) and BioNano Health-Guard Research Center funded by the MSIP of Korea as a Global Frontier Project (H-GUARD\_2013M3A6B2078947). This research was also supported by the Pioneer Research Center Program through the National Research Foundation of Korea funded by the MSIP (NRF-2012-0009586).

## Notes and references

- 1 A. Kumar, S. Kim and J.-M. Nam, *J. Am. Chem. Soc.*, 2016, **138**, 14509–14525.
- 2 J. Dong, Z. Zhang, H. Zheng and M. Sun, *Nanophotonics*, 2015, **4**, 1–19.
- 3 M. Li, S. K. Cushing and N. Wu, *Analyst*, 2015, **140**, 386–406.
- 4 S. T. Kochuveedu and D. H. Kim, *Nanoscale*, 2014, **6**, 4966–5019.
- 5 C. Zhou, S. Yang, J. Liu, M. Yu and J. Zheng, *Exp. Biol. Med.*, 2013, **238**, 1199–1209.
- 6 K. H. Drexhage, *Prog. Opt.*, 1974, **12**, 163–232.
- 7 C. D. Geddes and J. R. Lakowicz, *J. Fluoresc.*, 2002, **12**, 121–129.
- 8 J. Li, A. V. Krasavin, L. Webster, P. Segovia, A. V. Zayats and D. Richards, *Sci. Rep.*, 2016, **6**, 21349.
- 9 K. Ray, R. Badugu and J. R. Lakowicz, *J. Am. Chem. Soc.*, 2006, **128**, 8998–8999.
- 10 A. Mooradian, *Phys. Rev. Lett.*, 1969, **22**, 185–187.
- 11 J. R. Lakowicz, *Anal. Biochem.*, 2005, **337**, 171–194.
- 12 J. B. Khurgin, *Nat. Nanotechnol.*, 2015, **10**, 2–6.
- 13 D. A. Weitz, S. Garoff, J. I. Gersten and A. Nitzan, *J. Chem. Phys.*, 1983, **78**, 5324–5338.
- 14 D. Punj, M. Mivelle, S. B. Moparthy, T. S. van Zanten, H. Rigneault, N. F. van Hulst, M. F. García-Parajó and J. Wenger, *Nat. Nanotechnol.*, 2013, **8**, 512–516.
- 15 F. Benz, M. K. Schmidt, A. Dreismann, R. Chikkaraddy, Y. Zhang, A. Demetriadou, C. Carnegie, H. Ohadi, B. de Nijs, R. Esteban, J. Aizpurua and J. J. Baumberg, *Science*, 2016, **354**, 726–729.
- 16 R. Chikkaraddy, B. de Nijs, F. Benz, S. J. Barrow, O. A. Scherman, E. Rosta, A. Demetriadou, P. Fox, O. Hess and J. J. Baumberg, *Nature*, 2016, **535**, 127–130.
- 17 C. Tserkezis, R. Esteban, D. O. Sigle and J. Mertens, *Phys. Rev. A*, 2015, **92**, 053811.
- 18 G. M. Akselrod, *Nat. Photonics*, 2014, **8**, 835–840.
- 19 T. B. Hoang, G. M. Akselrod, C. Argyropoulos, J. Huang, D. R. Smith and M. H. Mikkelsen, *Nat. Commun.*, 2015, **6**, 8788.
- 20 H. Takata, H. Naiki, L. Wang, H. Fujiwara, K. Sasaki, N. Tamai and S. Masuo, *Nano Lett.*, 2016, **16**, 5770–5778.
- 21 S. Khatua, P. M. R. Paulo, H. Yuan, A. Gupta, P. Zijlstra and M. Orrit, *ACS Nano*, 2014, **8**, 4440–4449.
- 22 N. S. Abadeer, M. R. Brennan, W. L. Wilson and C. J. Murphy, *ACS Nano*, 2014, **8**, 8392–8406.
- 23 D. Punj, R. Regmi, A. Devilez, R. Plauchu, S. B. Moparthy, B. Stout, N. Bonod, H. Rigneault and J. Wenger, *ACS Photonics*, 2015, **2**, 1099–1107.
- 24 A. Puchkova, C. Vietz, E. Pibiri, B. Wünsch, M. Sanz Paz, G. P. Acuna and P. Tinnefeld, *Nano Lett.*, 2015, **15**, 8354–8359.
- 25 D.-K. Lim, K.-S. Jeon, J.-H. Hwang, H. Kim, S. Kwon, Y. D. Suh and J.-M. Nam, *Nat. Nanotechnol.*, 2011, **6**, 452–460.
- 26 C. Ayala-Orozco, J. G. Liu, M. W. Knight, Y. Wang, J. K. Day, P. Nordlander and N. J. Halas, *Nano Lett.*, 2014, **14**, 2926–2933.
- 27 J.-E. Park, S. Kim, J. Son, Y. Lee and J.-M. Nam, *Nano Lett.*, 2016, **16**, 7962–7967.
- 28 J.-M. Nam, J.-W. Oh, H. Lee and Y. D. Suh, *Acc. Chem. Res.*, 2016, **49**, 2746–2755.
- 29 T. Zhang, G. Lu, W. Li, J. Liu, L. Hou, P. Perriat, M. Martini, O. Tillement and Q. Gong, *J. Phys. Chem. C*, 2012, **116**, 8804–8812.
- 30 I. G. Theodorou, Z. A. R. Jawad, H. Qin, E. O. Aboagye, A. E. Porter, M. P. Ryan and F. Xie, *Nanoscale*, 2016, **8**, 12869–12873.





- 31 B. Zhou, B. Shi, D. Jin and X. Liu, *Nat. Nanotechnol.*, 2015, **10**, 924–936.
- 32 Y. Wang, F. Nan, Z. Cheng, J. Han, Z. Hao, H. Xu and Q. Wang, *Nano Res.*, 2015, **8**, 2970–2977.
- 33 Y. Li, J. Tang, L. He, Y. Liu, Y. Liu, C. Chen and Z. Tang, *Adv. Mater.*, 2015, **27**, 4075–4080.
- 34 N. J. Greybush, M. Saboktakin, X. Ye, C. Della Giovampaola, S. J. Oh, N. E. Berry, N. Engheta, C. B. Murray and C. R. Kagan, *ACS Nano*, 2014, **8**, 9482–9491.
- 35 B. Zhao, N. Qi, K.-Q. Zhang and X. Gong, *Phys. Chem. Chem. Phys.*, 2016, **18**, 15289–15294.
- 36 A. L. Feng, M. L. You, L. Tian, S. Singamaneni, M. Liu, Z. Duan, T. J. Lu, F. Xu and M. Lin, *Sci. Rep.*, 2015, **5**, 7779.
- 37 O. Planas, N. Macia, M. Agut, S. Nonell and B. Heyne, *J. Am. Chem. Soc.*, 2016, **138**, 2762–2768.
- 38 P. Apell, R. Monreal and S. Lundqvist, *Phys. Scr.*, 1988, **38**, 174–179.
- 39 L. L. T. Ngoc, J. Wiedemair, A. van den Berg and E. T. Carlen, *Opt. Express*, 2015, **23**, 5547–5564.
- 40 G. T. Boyd, T. Rasing, J. R. R. Leite and Y. R. Shen, *Phys. Rev. B: Condens. Matter Mater. Phys.*, 1984, **30**, 519–526.
- 41 M. B. Mohamed, V. Volkov, S. Link and M. A. El-Sayed, *Chem. Phys. Lett.*, 2000, **317**, 517–523.
- 42 E. Dulkeith, T. Niedereichholz, T. A. Klar and J. Feldmann, *Phys. Rev. B: Condens. Matter Mater. Phys.*, 2004, **70**, 205424.
- 43 H. Hu, H. Duan, J. K. W. Yang and Z. X. Shen, *ACS Nano*, 2012, **6**, 10147–10155.
- 44 J. T. Hugall and J. J. Baumberg, *Nano Lett.*, 2015, **15**, 2600–2604.
- 45 J. Mertens, M.-E. Kleemann, R. Chikkaraddy, P. Narang and J. J. Baumberg, *Nano Lett.*, 2017, **17**, 2568–2574.
- 46 K.-Q. Lin, J. Yi, J.-H. Zhong, S. Hu, B.-J. Liu, J.-Y. Liu, C. Zong, Z.-C. Lei, J. Aizpurua, X. Wang, R. E. N. Esteban and B. Ren, *Nat. Commun.*, 2017, **8**, 14891.
- 47 K. Q. Lin, J. Yi, S. Hu, J. J. Sun, J. T. Zheng, X. Wang and B. Ren, *ACS Photonics*, 2016, **3**, 1248–1255.
- 48 T. V. Shahbazyan, *Nano Lett.*, 2013, **13**, 194–198.
- 49 M. Yorulmaz, S. Khatua, P. Zijlstra, A. Gaiduk and M. Orrit, *Nano Lett.*, 2012, **12**, 4385–4391.
- 50 Y. Fang, W.-S. Chang, B. Willingham, P. Swanglap, S. Dominguez-Medina and S. Link, *ACS Nano*, 2012, **6**, 7177–7184.
- 51 W. Rao, Q. Li, Y. Wang, T. Li and L. Wu, *ACS Nano*, 2015, **9**, 2783–2791.
- 52 X. Wu, T. Ming, X. Wang, P. Wang, J. Wang and J. Chen, *ACS Nano*, 2010, **4**, 113–120.
- 53 C. Lumdee, B. Yun and P. G. Kik, *ACS Photonics*, 2014, **1**, 1224–1230.
- 54 B. Neupane, L. Zhao and G. Wang, *Nanoscale*, 2013, **13**, 4087–4092.
- 55 X. Wang, K. Braun, D. Zhang, H. Peisert, H. Adler, T. Chasse and A. J. Meixner, *ACS Nano*, 2015, **9**, 8176–8183.
- 56 D. Huang, C. P. Byers, L.-Y. Wang, A. L. Hoggard, B. Hoenne, S. Dominguez-Medina, S. Chen, W.-S. Chang, C. F. Landes and S. Link, *ACS Nano*, 2015, **9**, 7072–7079.
- 57 D. Sivun, C. Vidal, B. Munkhbat, N. Arnold, T. A. Klar and C. Hrelescu, *Nano Lett.*, 2016, **16**, 7203–7209.
- 58 G. F. Walsh and L. Dal Negro, *Nano Lett.*, 2013, **13**, 786–792.
- 59 S. M. Tabakman, L. Lau, J. T. Robinson, J. Price, S. P. Sherlock, H. Wang, B. Zhang, Z. Chen, S. Tangsombatvisit, J. A. Jarrell, P. J. Utz and H. Dai, *Nat. Commun.*, 2011, **2**, 466.
- 60 C. Niu, Q. Song, G. He, N. Na and J. Ouyang, *Anal. Chem.*, 2016, **88**, 11062–11069.
- 61 Y. Pang, Z. Rong, R. Xiao and S. Wang, *Sci. Rep.*, 2015, **5**, 9451–9458.
- 62 Z. Zheng and T. Majima, *Angew. Chem.*, 2016, **128**, 2929–2933.
- 63 G. Lu, L. Hou, T. Zhang, J. Liu, H. Shen, C. Luo and Q. Gong, *J. Phys. Chem. C*, 2012, **116**, 25509–25516.
- 64 J.-E. Park, M. Kim, J.-H. Hwang and J.-M. Nam, *Small Methods*, 2017, **1**, 1600032.
- 65 A. L. Antaris, H. Chen, K. Cheng, Y. Sun, G. Hong and C. Qu, *Nat. Mater.*, 2015, **15**, 235–242.
- 66 X. Ding, C. H. Liow, M. Zhang, R. Huang, C. Li, H. Shen, M. Liu, Y. Zou, N. Gao, Z. Zhang, Y. Li, Q. Wang, S. Li and J. Jiang, *J. Am. Chem. Soc.*, 2014, **136**, 15684–15693.

